

Lect. 10. Image Processing Methods in Digital Holography

10. IMAGE PERFECTING METHODS

Image perfecting is processing aimed at correcting image signal distortions introduced by imaging systems. In this chapter, we will give a brief review of image processing methods that are most relevant to digital holography. Specifically, we will review methods of noise reduction and methods of correction of distortions associated with aperture of scanning and display and hologram recording devices and distortions caused by nonlinearities in imaging and holographic devices.

10.1. Transform domain MSE optimal scalar Wiener Filters

In this section we first consider image restoration for an imaging system model that disregards point-wise nonlinear transformation in imaging systems and treats image distortions as a combination of only distortions caused by linear filtering and of those caused by action of random interferences.

The design of the optimal restoration procedure requires specifying a criterion for evaluating the restoration quality. Let $\{\mathbf{b}_k\}$ be a set of N signal samples ($k = 0, 1, \dots, N-1$) at the output of the imaging system, $\{\mathbf{a}_k\}$ be a set of the system's input signal samples that model a perfect, or "ideal" signal and $\{\hat{\mathbf{a}}_k\}$ be a set of restored signal samples. For the sake of generality, we will consider the set $\{\mathbf{a}_k\}$ as a realization taken from a statistical ensemble Ω_A or data base of input signals and the set $\{\mathbf{b}_k\}$ as a realization of a signal ensemble generated by ensembles Ω_A and Ω_N of input signals and of random interferences, correspondingly.

Define the restoration procedure performance measure as a squared difference between restored and perfect signals averaged over the available set of signal samples and over statistical ensembles Ω_A and Ω_N . We will call this measure *mean squared restoration error* (MSE). The restoration procedure $\mathbf{R}\{\mathbf{b}_k\} = \{\hat{\mathbf{a}}_k\}$ that minimizes this difference:

$$\{\hat{\mathbf{a}}_k\} = \underset{\mathbf{R}\{\mathbf{b}_k\}=\{\hat{\mathbf{a}}_k\}}{\mathbf{arg\,min}} \left\{ \mathbf{AV}_{\Omega_A} \mathbf{AV}_{\Omega_N} \left(\sum_{k=0}^{N-1} |\mathbf{a}_k - \hat{\mathbf{a}}_k|^2 \right) \right\}. \quad (10.1)$$

will be referred to as *MSE-optimal filtering*.

For the implementation of the MSE-optimal filtering, we will restrict ourselves to linear filtering. In general, linear filtering of a discrete signal can be described in a matrix form as multiplication of a vector of input signal samples $\mathbf{B} = \{\mathbf{b}_k\}$ by a filter matrix \mathbf{H} :

$$\hat{\mathbf{A}} = \mathbf{H} \cdot \mathbf{B}, \quad (10.2)$$

where $\hat{\mathbf{A}} = \{\hat{\mathbf{a}}_k\}$ is a vector of filter output signal samples

For signals of N samples, a general vector filter matrix \mathbf{H} has dimensions $N \times N$. Specification of such a filter requires determining N^2 filter coefficients, and

the filtering itself requires performing $O(N^2)$ operations per $O(N)$ signal samples, or N operation per sample. In image processing, the computational complexity of both determination of filter coefficients and of the filtering may be become too high because of high dimensionality of image arrays. Luckily, Fast transforms are available that may be computed for $O(\log N)$ operations per sample, which allows to radically decrease the filter design and the implementation complexity. Therefore in what follows we will consider only scalar filtering in a domain of orthogonal transforms that can be computed with fast algorithms. This class of filters is described by the equation:

$$\hat{\mathbf{A}} = \mathbf{T}^{-1} \cdot \mathbf{H}_d \cdot \mathbf{T} \cdot \mathbf{B}, \quad (10.3)$$

where, \mathbf{T} and \mathbf{T}^{-1} are, correspondingly, direct and inverse orthogonal transform matrices, $\mathbf{H} = \text{diag}\{\eta_r\}$, ($r = 0, 1, \dots, N-1$) is a diagonal filter matrix. Such a scalar filtering implies the following relationship between filter output and input signal samples $\{\hat{\alpha}_r\} = \mathbf{T} \cdot \hat{\mathbf{A}}$ and $\{\beta_r\} = \mathbf{T} \cdot \mathbf{B}$:

$$\hat{\alpha}_r = \eta_r \beta_r. \quad (10.4)$$

In the assumption of orthogonality of the transform \mathbf{T} , one can, by virtue of the Parseval relationship, modify the filter optimality condition defined by Eq. 10.1 in the following way:

$$\{\hat{\alpha}_r\} = \underset{\{\eta_r\}}{\text{arg min}} \left\{ \mathbf{A} \mathbf{V}_{\Omega_A} \mathbf{A} \mathbf{V}_{\Omega_N} \left(\sum_{r=0}^{N-1} |\alpha_r - \hat{\alpha}_r|^2 \right) \right\} = \underset{\{\eta_r\}}{\text{arg min}} \left\{ \mathbf{A} \mathbf{V}_{\Omega_A} \mathbf{A} \mathbf{V}_{\Omega_N} \left(\sum_{r=0}^{N-1} |\alpha_r - \eta_r \beta_r|^2 \right) \right\} \quad (10.5)$$

By computing derivatives over sought variables and equaling them to zero, one can obtain from Eq. 10.5 that optimal scalar filter coefficients are cross-correlation coefficients between spectral coefficients β_r and α_r of the input and perfect signals ([1]):

$$\eta_r = \frac{\mathbf{A} \mathbf{V}_{\Omega_A} \mathbf{A} \mathbf{V}_{\Omega_N} (\alpha_r \beta_r^*)}{\mathbf{A} \mathbf{V}_{\Omega_A} \mathbf{A} \mathbf{V}_{\Omega_N} (|\beta_r|^2)}. \quad (10.6)$$

MSE optimal linear filters and, in particular, MSE optimal scalar filters defined by Eq. 10.6 are commonly called *Wiener filters*.

In order to implement optimal scalar Wiener filter, one should therefore know cross-correlation $\{\mathbf{A} \mathbf{V}_{\Omega_A} \mathbf{A} \mathbf{V}_{\Omega_N} (\alpha_r \beta_r^*)\}$ between filter input signal and perfect signal spectral coefficients and power spectrum $\{\mathbf{A} \mathbf{V}_{\Omega_A} \mathbf{A} \mathbf{V}_{\Omega_N} (|\beta_r|^2)\}$ of the input signal in the selected basis. The statistical approach we adopted assumes averaging of the restoration error over statistical ensembles of perfect signals and of filter input signals. This implies that the required statistical parameters should be measured in advance for these ensembles or over the data bases.

10.2. Filtering additive signal independent noise and empirical Wiener filters

Consider a noise model, in which filter input signal samples $\{b_k\}$ are obtained as a sum of perfect signal samples $\{a_k\}$ and samples $\{n_k\}$ of signal independent zero mean random noise:

$$b_k = a_k + n_k. \quad (10.7)$$

In spectral domain, the same relationship holds for signal and noise spectral coefficients:

$$\beta_r = \alpha_r + \nu_r, \quad (10.8)$$

where $\{\nu_r\} = \mathbf{T}\{n_k\}$. For this model one can obtain that

$$\text{AV}_{\Omega_A} \text{AV}_{\Omega_N}(\alpha_r \beta_r^*) = \text{AV}_{\Omega_A} \text{AV}_{\Omega_N}[\alpha_r (\alpha_r^* + \nu_r^*)] = \text{AV}_{\Omega_A}(|\alpha_r|^2) \quad (10.9)$$

and

$$\text{AV}_{\Omega_A} \text{AV}_{\Omega_N}(|\beta_r|^2) = \text{AV}_{\Omega_A} \text{AV}_{\Omega_N}[(\alpha_r + \nu_r)(\alpha_r^* + \nu_r^*)] = \text{AV}_{\Omega_A}(|\alpha_r|^2) + \text{AV}_{\Omega_N}(|\nu_r|^2) \quad (10.10)$$

because for zero mean noise $\text{AV}_{\Omega_N}(\nu_r^*) = \text{AV}_{\Omega_N}(\nu_r) = 0$. Therefore scalar Wiener filter for suppressing additive signal independent noise is defined through its coefficients $\{\eta_r\}$ as

$$\eta_r = \frac{\text{AV}_{\Omega_A}(|\alpha_r|^2)}{\text{AV}_{\Omega_A}(|\alpha_r|^2) + \text{AV}_{\Omega_N}(|\nu_r|^2)}. \quad (10.11)$$

One can give to this formula a clear physical interpretation. Define *signal-to-noise ratio* as:

$$\text{SNR}_r = \frac{\text{AV}_{\Omega_A}(|\alpha_r|^2)}{\text{AV}_{\Omega_N}(|\nu_r|^2)}. \quad (10.12)$$

Then obtain:

$$\eta_r = \frac{\text{SNR}_r}{1 + \text{SNR}_r}, \quad (10.13)$$

which means that scalar Wiener filter weight coefficients are defined, for each signal spectral coefficient, by the signal-to-noise ratio for this coefficient. The lower is signal-to-noise ratio for a particular signal spectral component, the lower the contribution of this component to the filter output signal.

In order to implement scalar Wiener filter one has to know in advance power spectra $\text{AV}_{\Omega_A}(|\alpha_r|^2)$ and $\text{AV}_{\Omega_N}(|v_r|^2)$ of perfect signals and of noise in the selected basis. Noise power spectrum may be known from the specification certificate of the imaging device. Otherwise it can be measured in noisy input signals using methods described in Lect. 9. As for the perfect signal power spectrum, it is most frequently not known. However, one can, using Eq. 10.10, attempt to estimate it from the power spectrum $\text{AV}_{\Omega_A} \text{AV}_{\Omega_N}(|\beta_r|^2)$ of input noisy signals as

$$\text{AV}_{\Omega_A}(|\alpha_r|^2) = \text{AV}_{\Omega_A} \text{AV}_{\Omega_N}(|\beta_r|^2) - \text{AV}_{\Omega_A}(|v_r|^2). \quad (10.14)$$

The latter has to be estimated from the observed signal spectrum $|\beta_r|^2$. Denote this estimate as $\overline{|\beta_r|^2}$. This empirical estimate made by averaging over available realization of input images may, when used as a replacement for $\text{AV}_{\Omega_A} \text{AV}_{\Omega_N}(|\beta_r|^2)$, give negative values for some spectral coefficients because of the limited depth of the averaging. Since power spectra cannot assume negative values, the following modified spectrum estimation may be adopted:

$$\text{AV}_{\Omega_A}(|\alpha_r|^2) = \max\left[\overline{|\beta_r|^2} - \text{AV}_{\Omega_A}(|v_r|^2); \mathbf{0}\right]. \quad (10.15)$$

In this way we arrive at the filter:

$$\eta_r = \max\left[\frac{\overline{|\beta_r|^2} - \text{AV}_{\Omega_A}(|v_r|^2)}{\overline{|\beta_r|^2}}; \mathbf{0}\right]. \quad (10.16)$$

We will refer to this filter as the *empirical Wiener filter*.

If the imaging system noise is known to be white noise with variance σ_{noise}^2 , the empirical Wiener filter takes the form:

$$\eta_r = \max\left[\frac{\overline{|\beta_r|^2} - \sigma_{noise}^2}{\overline{|\beta_r|^2}}; \mathbf{0}\right]. \quad (10.17)$$

As a zero order approximation to the input images power spectrum, power spectrum $|\beta_r|^2$ of a single input image subjected to filtering may be used. In this case empirical Wiener filter weight coefficients are found as:

$$\eta_r = \max\left[\frac{|\beta_r|^2 - \sigma_n^2}{|\beta_r|^2}; \mathbf{0}\right]. \quad (10.18)$$

Note that such an empirical Wiener filter is adaptive because its weight coefficients depend on the spectrum of the image to which it will be applied.

Weight coefficients of scalar Wiener filters assume values in the range between zero and one. A version of the empirical Wiener filter of Eq. 10.18 with binary weight coefficients:

$$\eta_r = \begin{cases} 1, & \text{if } |\beta_r|^2 \geq Thr \\ 0, & \text{otherwise} \end{cases}, \quad (10.19)$$

where Thr is a rejecting threshold, is called the *rejecting filter*. As it follows from Eq. 10.18, the rejecting threshold has a value of the order of magnitude of the noise variance σ_n^2 . Rejecting filters eliminate from the input images spectra all components for which signal-to-noise ratio is lower than a certain threshold commensurable with the noise variance.

Described empirical Wiener filters for signal denoising are particularly very efficient if signal and/or noise spectra are well concentrated and are separated in the transform domain selected for processing. A typical example of such a situation is filtering of quasi-periodical noise interferences, whose spectrum has only a few components in the domain of Discrete Fourier (DFT) or Discrete Cosine (DCT) Transforms. Such interferences frequently appear, for instance, in images digitized by frame grabbers from analog video. Fig. 10.1 demonstrates filtering quasi-periodical noise pattern in an image. Left column in Fig. 10.1 shows input and filtered images. Right column shows averaged spectra of input and output image rows.

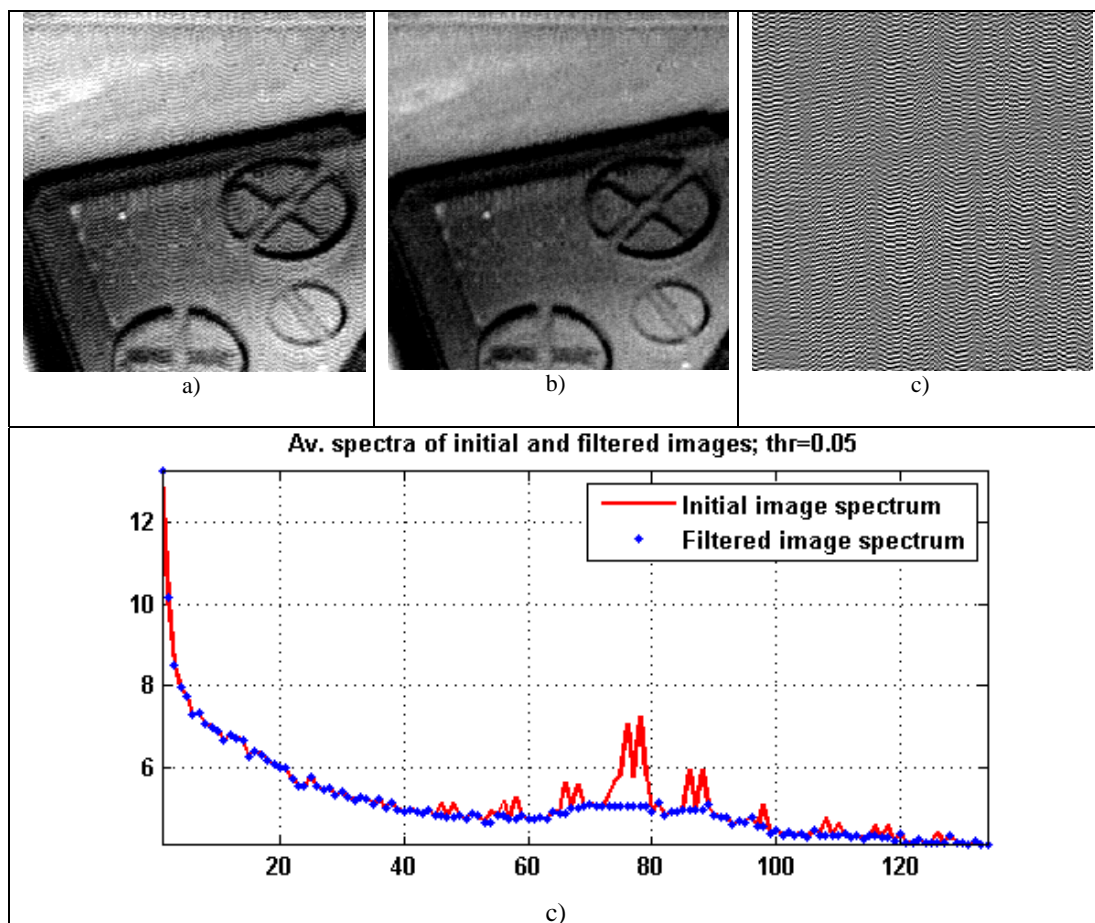


Figure 10.1. Filtering periodic interferences: a) initial noisy image; b) filtered image; c) difference between noisy and filtered images; d) DFT spectra of initial and noisy images

One can clearly see anomalous peaks of noise spectrum in input image spectrum that are eliminated in the output image spectrum after applying empirical Wiener filtering designed using methods of noise spectrum estimation described in Lect. 9. Note that the filtering is carried out in this example as 1-D row-wise filtering in DFT domain.

Fig. 10.2 illustrates similar 2-D rejecting filtering for eliminating periodical noise components in a digitized Fresnel hologram.

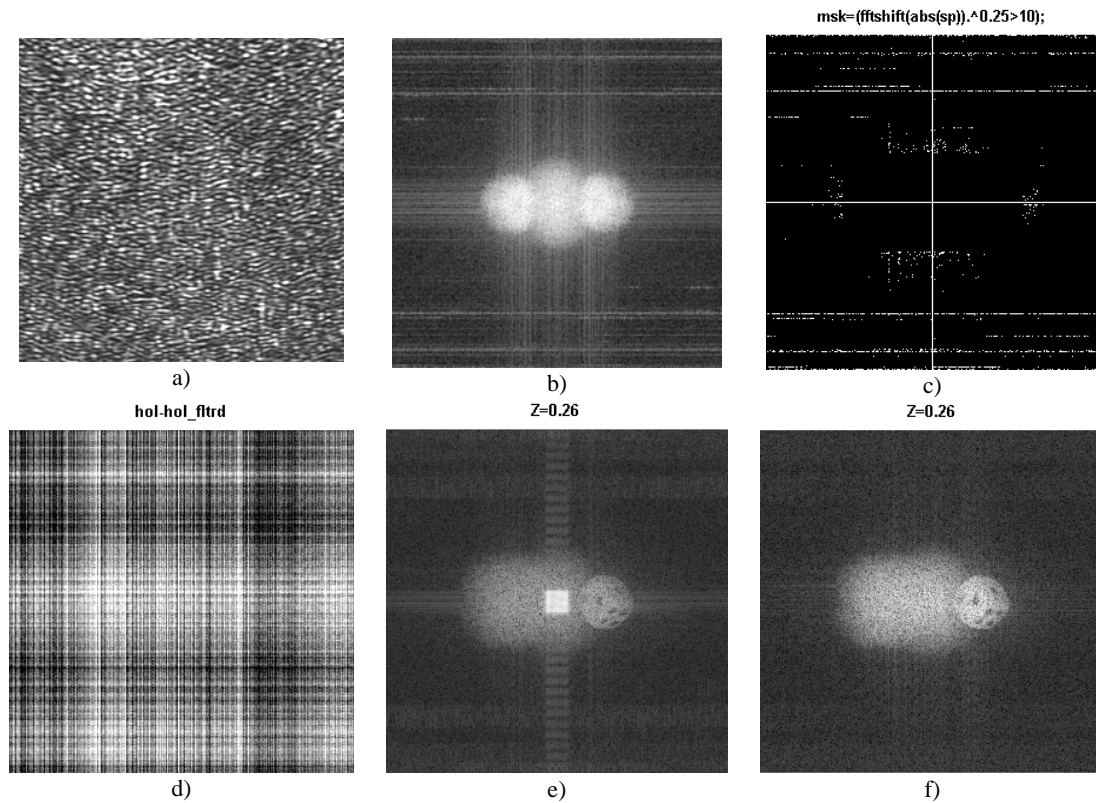


Figure 10.2. Prior reconstruction cleaning quasi-periodic interferences in Fresnel holograms: a) a digitized hologram; b) DFT spectrum of the hologram, which striation reveals the presence of quasi-periodic interference; c) pattern of 2-D rejecting filter coefficients (black for 1 and white for 0); d) difference between initial hologram and filtered one demonstrating noise pattern removed by the filtering; e) image reconstructed from the initial hologram; f) image reconstructed from the filtered hologram, which shows removal of interferences seen in figure e). (The hologram was kindly granted by Dr. T. Kraus, BIAS, Bremen, Germany)

Fig. 10.3 shows yet another example of empirical Wiener filtering, this time filtering linear striation interferences. Linear striation interference in the initial image shown in Fig. 10.3 is characteristic for imaging systems with mechanical scanning. This particular image was produced by an atomic force microscope. Striation interference randomly distorts image dc component (row-wise mean value) in the direction of scanning. Upper right plot in Fig. 10.3 shows row-wise mean values (horizontal coordinate), which can be regarded as row-wise image Radon transform, as a function of the row number (vertical coordinate). Taking as an estimate of perfect mean row-wise values a mean value over all rows (shown with a straight line in the bottom right plot in Fig. 10.3), one can estimate the striation interference on every row by subtracting this estimate from the observed mean values. Subtracting the found values from all pixels in the corresponding row eliminates the interference.

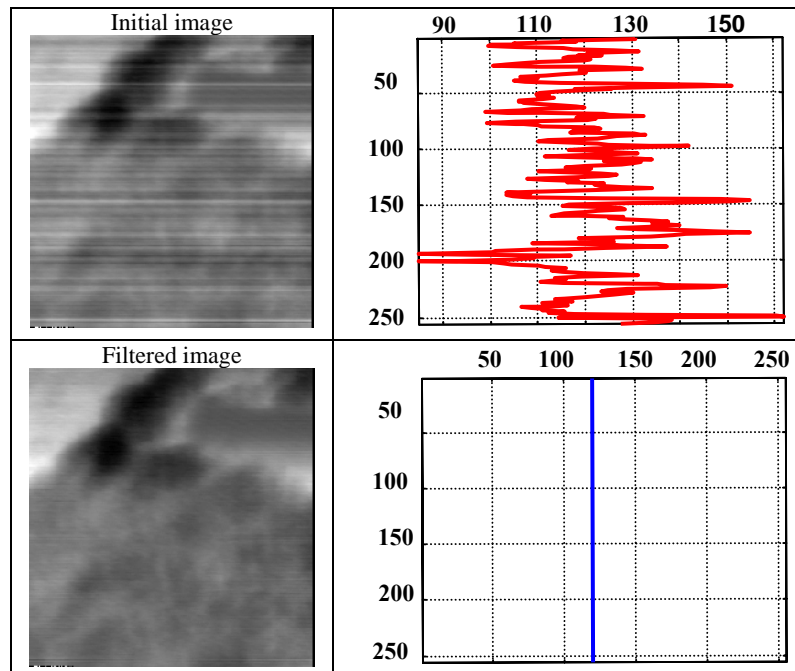


Figure 10.3. Filtering linear striation interference

The same principle can be applied to filtering wide band noise in interferograms recorded with a spatial carrier. In this case useful signal of interferogram is very narrow-band in the domain of DFT or DCT, whereas noise spectrum is spread uniformly over entire spectral plane. Upon detecting in Fourier domain peak of the spectrum of the interferogram using methods described in Lect. 9, one can synthesize an empirical Wiener or a rejecting filter and then apply it to the noisy interferogram. A result of such processing is illustrated in Fig. 10.4.

In image processing applications, Wiener filtering of wide band noise and especially white noise in images is less efficient than in filtering narrow-band noise. When filtering of white noise, Wiener filter tends to weaken low energy signal spectral components. However usually these components are exactly the components that are the most important in images because they carry information about signal changes such as at edges in images. Moreover, Wiener filtering converts input white noise into correlated output residual noise, though with a reduced variance. As one can see from Eq. 10.11, in case of the intensive input white noise, power spectrum of the residual noise is roughly proportional to the signal power spectrum which means that the residual noise becomes, statistically, signal alike. This may substantially hamper subsequent image visual analysis. In particular, it is well known that human vision is more sensitive to correlated noise than to white noise of the same intensity. Therefore Wiener filtering for image denoising may even worsen image visual quality.

A version of the empirical Wiener filter and of the rejecting filters that are implemented with wavelet transform image decomposition is known as *wavelet shrinkage* filtering ([3]). Empirical Wiener filtering according to Eq. 10.18 is called on a wavelet jargon “*soft thresholding*”. Rejecting filtering according to Eq. 10.19 is called “*hard thresholding*”. Fig. 10.5 shows flow diagram of signal denoising by the wavelet shrinkage.

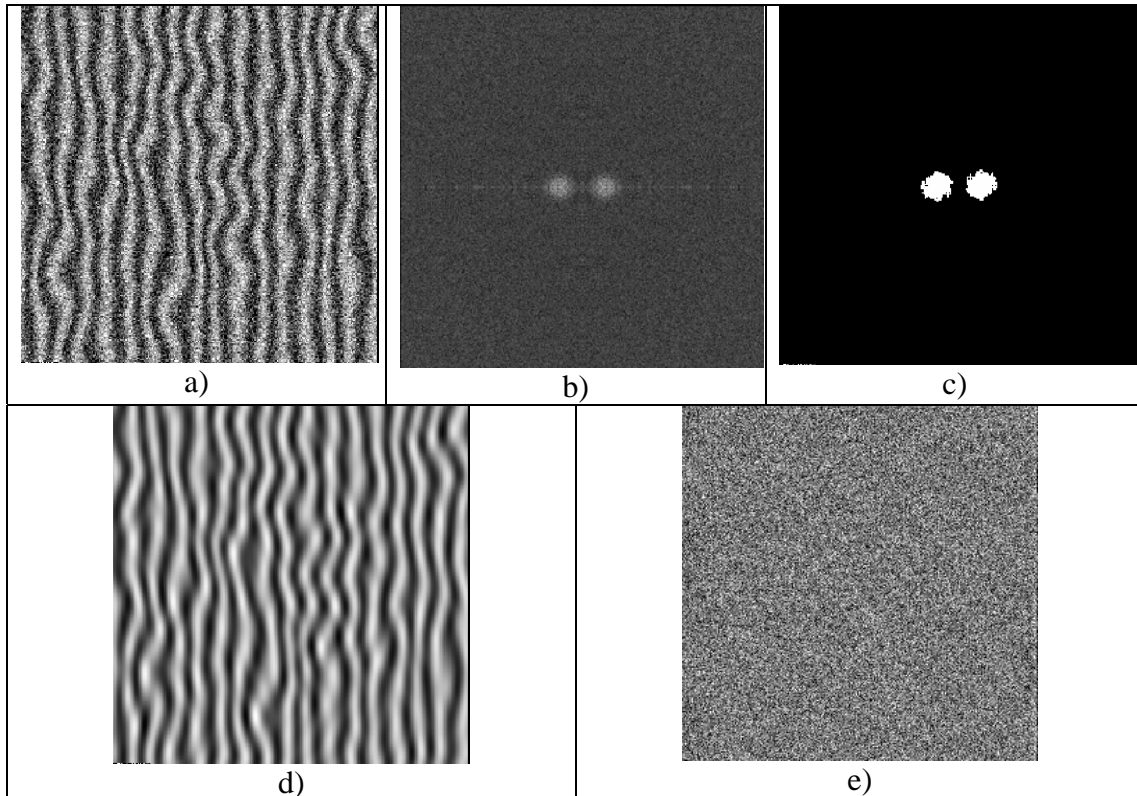


Fig. 10.4. Denoising interferogram using a rejecting filter: a) noisy interferogram; b) 2D DFT spectrum of the noisy interferogram; c) rejecting filter frequency response in DFT domain (white areas are frequencies, where filter frequency response is one, black areas are frequencies, where filter frequency response is zero); d) filtering result; e) difference between noisy interferogram and the filtered one, which presents noise removed from the interferogram.

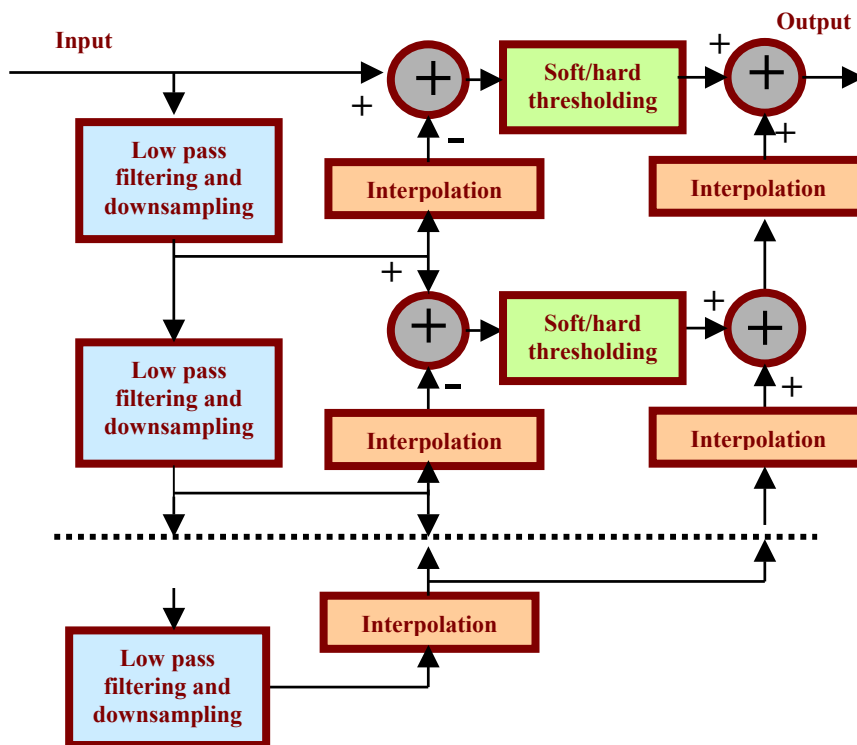


Figure 10.5 Wavelet shrinkage: signal denoising in wavelet transform domain

10.3. Image deblurring, inverse filters and aperture correction.

Consider now an imaging system model that accounts also for signal linear transformations in imaging systems. Suppose that the linear transformation unit can be modeled as a scalar filter with filter coefficients $\{\lambda_r\}$ in a selected basis. For DFT and DCT bases, this assumption is justified, to the accuracy of boundary effects, for shift invariant linear filtering. In this case coefficients $\{\lambda_r\}$ are samples of imaging system frequency response. In ideal imaging systems, they should all be equal to unity. In reality, they decay with the frequency index r , which results, in particular, in image blur. Processing aimed at correcting this type of distortions is frequently referred to as *image deblurring*.

For such systems, we have in the transform domain:

$$\beta_r = \lambda_r \alpha_r + v_r, \quad (10.20)$$

Using Eqs. 10.6, one can obtain that the scalar Wiener image restoration filter is defined in this case by the equation ([1]):

$$\eta_r = \frac{1}{\lambda_r} \frac{SNR_r}{1 + SNR_r}, \quad (10.21)$$

where SNR is signal-to-noise ratio at the output of the linear filter unit of the imaging system model:

$$SNR_r = \frac{|\lambda_r|^2 \text{AV}_{\Omega_A}(|\alpha_r|^2)}{\text{AV}_{\Omega_N}(|v_r|^2)}. \quad (10.22)$$

Correspondingly, the general empirical Wiener filter, empirical Wiener filter with zero order approximation to perfect signal spectrum and the rejecting filter for aperture correcting and image deblurring will be in this case as follows:

$$\eta_r = \max \left[\frac{1}{\lambda_r} \frac{\overline{|\beta_r|^2} - \text{AV}_{\Omega_A}(|v_r|^2)}{\overline{|\beta_r|^2}}; \mathbf{0} \right]; \quad (10.23)$$

$$\eta_r = \max \left[\frac{1}{\lambda_r} \frac{\overline{|\beta_r|^2} - \sigma_n^2}{\overline{|\beta_r|^2}}; \mathbf{0} \right] \quad (10.24)$$

and

$$\eta_r = \begin{cases} \frac{1}{\lambda_r}, & \text{if } |\beta_r|^2 \geq Thr \\ \mathbf{0}, & \text{otherwise} \end{cases}. \quad (10.25)$$

All these filters may be treated as two filters in cascade: the filter with coefficients

$$\eta_r^{inv} = \frac{1}{\lambda_r} \quad (10.26)$$

usually called the *inverse filter* and signal denoising filters described by Eqs. 10.17 - 19.

Inverse filters compensate weakening signal frequency components in the imaging system while denoising filters prevent from excessive amplification of noise and perform what is called “*regularization*” of inverse filters. As one can see from Eq. 10.22, weight coefficients of denoising filters for small $\{\lambda_r\}$ decay faster than weight coefficients of the inverse filter grow.

One of the most immediate applications of inverse filters is correcting distortions caused by finite size of apertures of image sensors, image sampling devices and image displays. We will refer to this processing as *aperture correction*.

Let an image sensor and discretization device is an array of light sensitive elements with a square aperture of size $d^{(s)} \times d^{(s)}$ (Fig. 10.6). Then frequency response of the individual sensor elements is

$$H(f_x, f_y) = \int_{-d^{(s)}/2}^{d^{(s)}/2} \exp(i2\pi f_x x) dx \int_{-d^{(s)}/2}^{d^{(s)}/2} \exp(i2\pi f_y y) dy =$$

$$\frac{\sin(\pi f_x d^{(s)}/2)}{\pi f_x d^{(s)}/2} \frac{\sin(\pi f_y d^{(s)}/2)}{\pi f_y d^{(s)}/2} = \text{sinc}(\pi f_x d^{(s)}) \text{sinc}(\pi f_y d^{(s)}), \quad (10.27)$$

or, in dimensionless coordinates $\{\bar{f}_x = f_x \Delta x, \bar{f}_y = f_y \Delta x\}$, where Δx is the sampling interval in both coordinates,

$$H(\bar{f}_x, \bar{f}_y) = \text{sinc}(\pi \bar{f}_x d^{(s)} / \Delta x) \text{sinc}(\pi \bar{f}_y d^{(s)} / \Delta x). \quad (10.28)$$

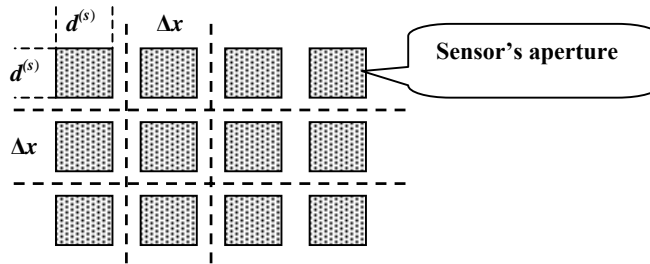


Figure 10.6 Arrangement of light sensitive elements in image sensor arrays

The discrete frequency response of the sensor is then:

$$\lambda_{r,s} = \lambda_r \lambda_s = \text{sinc}(\pi \bar{d}^{(s)} \lambda_r / N_x) \cdot \text{sinc}(\pi \bar{d}^{(s)} \lambda_s / N_y), \quad (10.29)$$

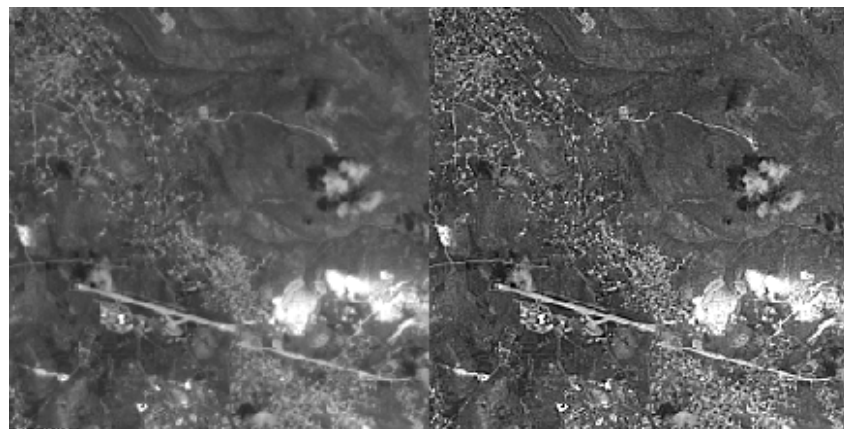
where $\bar{d}^{(s)} = d^{(s)} / \Delta x$.

If the image display device has also a square aperture of size $d^{(r)} \times d^{(r)}$, the overall imaging discrete system frequency response is:

$$\lambda_{r,s} = \lambda_r \lambda_s = \text{sinc}(\pi \bar{d}^{(s)} \lambda_r / N_x) \cdot \text{sinc}(\pi \bar{d}^{(r)} \lambda_r / N_x) \times \text{sinc}(\pi \bar{d}^{(s)} \lambda_s / N_y) \text{sinc}(\pi \bar{d}^{(r)} \lambda_s / N_y). \quad (10.30)$$

Parameters $\bar{d}^{(s)}$, $\bar{d}^{(r)}$ and Δx are imaging system design parameters that may be known from system's certificate. They can be used for correcting image distortions by processing images in computer.

Fig. 10.7 illustrates an example of the aperture correction of an air photograph. Right image in this figure is obtained by applying to the left image an inverse filter for the system's frequency response defined by Eq. 10.20 with $\bar{d}^{(s)} = \bar{d}^{(r)} = 1$.



Initial (left) and aperture corrected (right) images

Figure 10.7. Aperture correction: initial (left) and aperture corrected (right) images

In synthesis of computer-generated holograms, aperture correction is required to compensate masking images reconstructed from holograms by the frequency response of the hologram recording device (see Lect. 6). This masking may result in substantial reducing image contrast on the periphery of image plane. The aperture correction can be implemented by multiplying object image, before the hologram computation, by the function inverse to the hologram recording device frequency response. This method is illustrated in Fig. 10.8.

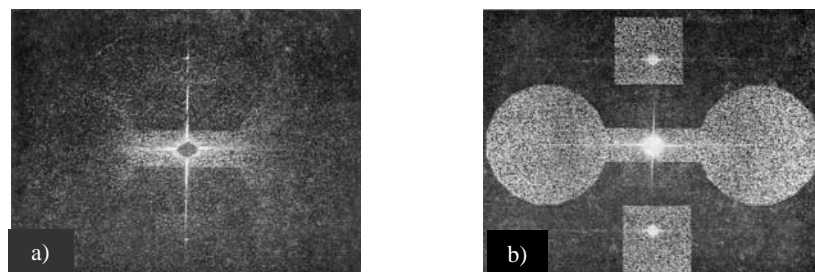


Figure 10.8. Effect of spatial masking of reconstructed images due to the finite size of the hologram recording aperture (a) and the result of its compensation (b) (adopted from [4])

10.4. Local adaptive filtering

In the derivation of the MSE optimal scalar linear filters, the size of input signal vectors was a free parameter. In the filter implementation, one should select the fashion, in which signals are to be processed. Given an image to be processed, filtering can be designed and carried out either over the entire set of available image samples or fragment-wise. We will refer to the former as *global filtering* and to the latter as *local filtering*.

There is a number of arguments in favor of "local" filtering versus "global" one:

- "Global" filtering assumes signal "stationarity" or spatial homogeneity. For scalar linear filtering, this means signal homogeneity in terms of signal power spectra: spectra measured over different signal fragments should not substantially deviate one from another. In many applications, one can hardly regard images as being spatially homogeneous.
- Adaptive filter design assumes empirical evaluation of signal spectra. Global evaluation of image spectrum disregards spectra variations due to image inhomogeneity. This obviously results in neglecting local image information in favor of global one, which usually contradicts processing goals.
- Objects to be recognizable visually have to contain sufficiently large number of resolution cells (pixels). As an immediate illustration of this fact one can recall that, for the reproduction of printed characters, one needs a array of at least 8x8 or more pixels. The same and even to a greater degree holds for "texture" images. Texture identification is also possible only if texture area contains sufficiently large numbers of pixels. This means that image can be regarded as a composition of object domains with the linear size from several to several tens of resolution cells.
- It is well known that when viewing image, eye optical axis permanently jumps "randomly" over the field of view. Human visual acuity is very uneven over the field of view. The field of view of the human vision is about 40°-60°. Resolving power of the vision is about one angular minute. However such a relatively high resolving power is concentrated only within a small fraction of the field of view that has size of about 2° ([5]). Therefore, the area of acute vision is about 1/30-th to 1/20-th of the field of view. For images of 512x512pixels this means window of roughly from 17x17 to 25x25 pixels.

A theoretical framework for local filtering is provided by local criteria of processing quality ([1]). For optimal local MSE scalar filters, filter coefficients $\{\eta_r^{(k)}\}$ are, according to the local criteria, defined by the equation:

$$\hat{\alpha}_r^{(k)} = \arg \min_{\{\eta_r\}} \left\{ \mathbf{AV}_{\Omega_A} \mathbf{AV}_{\Omega_N} \left(\sum_{r=0}^{W-1} |\alpha_r^{(k)} - \eta_r^{(k)} \beta_r^{(k)}|^2 \right) \right\}, \quad (10.31)$$

where W is it the filter window size and, correspondingly, the size of the area over which filtering performance is evaluated, k is an index of the window position on the sampling grid, $\{\beta_r^{(k)}\}$ are spectral coefficients of the filter input samples within the filter window, $\{\alpha_r^{(k)}\}$ are spectral coefficients of hypothetical perfect signal samples within the filter window. The solutions obtained above for empirical Wiener filters for image restoration may then be extended to local filtering by replacing in Eqs. 10.16 -

19 and 10.23-26 signal spectra with corresponding local spectra of the signal window samples.

The most straightforward way to implement local filtering is to perform it in a hopping window. This is exactly the way of processing implemented in most popular audio and image coding methods such as JPEG and MPEG. "Hopping window" processing being very attractive from the computational complexity point of view suffers however from "blocking effects" - artifacts in form of discontinuities at the edges of the hopping window. Obviously, an ultimate solution of the "blocking effects" problem would be sliding window processing. Sliding window filtering is local adaptive because, for empirical Wiener filters, filter coefficients depend on local spectra of image fragments.

In the sliding window filtering, one should, for each position of the filter window, compute transform coefficients of the input signal samples within window, design on this base the filter, modify accordingly transform coefficients and then compute inverse transform. With sliding window, inverse transform need not, in principle, be computed for all signal samples within the filter window since only the central sample of the window has to be determined in order to form the output signal in the process of image scanning with the filter window. Fig. 10.9 illustrates this process.

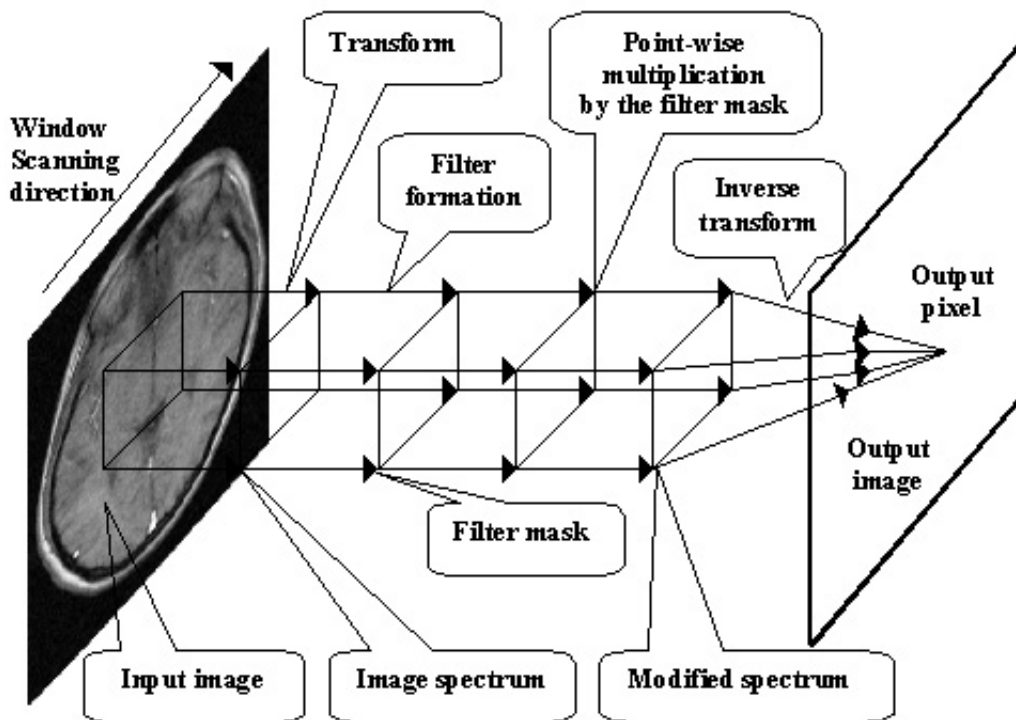


Figure 10.9. The principle of local adaptive filtering in sliding window

Selection of orthogonal transforms for implementation of local adaptive filtering is governed by

- the required accuracy of approximation of general linear filtering with scalar filtering;
- the convenience of formulating a priori knowledge regarding image spectra in the chosen transform domain;

- the accuracy of the empirical spectrum estimation from the observed data that is required for the adaptive filter design;
- the computational complexity of the filter implementation.

Among all known transforms, Discrete Cosine Transform proved to be one of the most appropriate transforms for sliding window transform domain filtering ([1,2]). DCT exhibits a very good energy compaction capability, which is a key feature for the efficiency of the filter design and implementation. Being advantageous to DFT in terms of the energy compaction capability, DCT can also be regarded as a good substitute for DFT in signal/image restoration tasks with imaging system specification in terms of their frequency responses. DCT is also quite suitable for multi component image processing. The use of DCT in sliding window has low computational complexity owing to the recursive algorithms for computing DCT in sliding windows ([1]). In addition note that, if the window size N_w is an odd number, the inverse DCT transform of local spectrum $\beta_r^{(k)}$ for computing window central pixel $a_{k+(N_w-1)/2}$ of the filter output

$$a_{k+(N_w-1)/2} = \beta_0^{(k)} + 2 \sum_{r=1}^{W-1} \beta_r^{(k)} \cos(\pi r / 2) = \beta_0^{(k)} + 2 \sum_{s=1}^{(W-1)/2} \beta_{2s}^{(k)} (-1)^s, \quad (10.32)$$

involves only signal spectrum coefficients with even indices. Therefore only those spectral coefficients have to be computed and the computational complexity of sliding window filtering in DCT domain is $O[(W+1)/2]$ operations for 1-D filtering and $O[(W+1)^2/4]$ operations for 2-D filtering in a square window of $W \times W$ pixels.

Fig. 10.10 illustrates local adaptive empirical Wiener filtering of a piece-wise constant test noisy image with noise dynamic range ± 20 gray levels of 256.

Upper left image is the initial test image. Upper right image is the input image with noise added. Left bottom image is the result of the filtering. Right bottom image shows residual noise in the filtered image as a difference between noise less image and filtered one. One can see from this image that the residual noise is observed practically only in the vicinity of the borders of piece wise constant patches of the test image. This means that when filter window seats on an image patch, where image gray values are constant, the filter is almost completely opaque and preserves only image local dc component (local mean) while on the patch boundaries the filter is almost fully transparent to signal spectral components and prefers not to remove noise in order to preserve edges of patches. This edge preserving capability is an important advantage of the local adaptive filtering comparing to the global filtering. It is interesting to note that similar insensitivity to noise in the vicinity of image edges is characteristic for human vision as well.

Local adaptive filtering allows also denoising images with signal dependent noise such as speckle noise. The characteristic feature of the speckle noise is that its standard deviation is proportional to the signal (see Lect. 9). For filtering speckle noise with local adaptive filters, one should set parameters σ_n and Thr of the filters of Eqs. 10.17 through 19 to be proportional to the image local mean component $\beta_0^{(k)}$. Fig. 10.11 shows an example of such denoising of an interferogram.

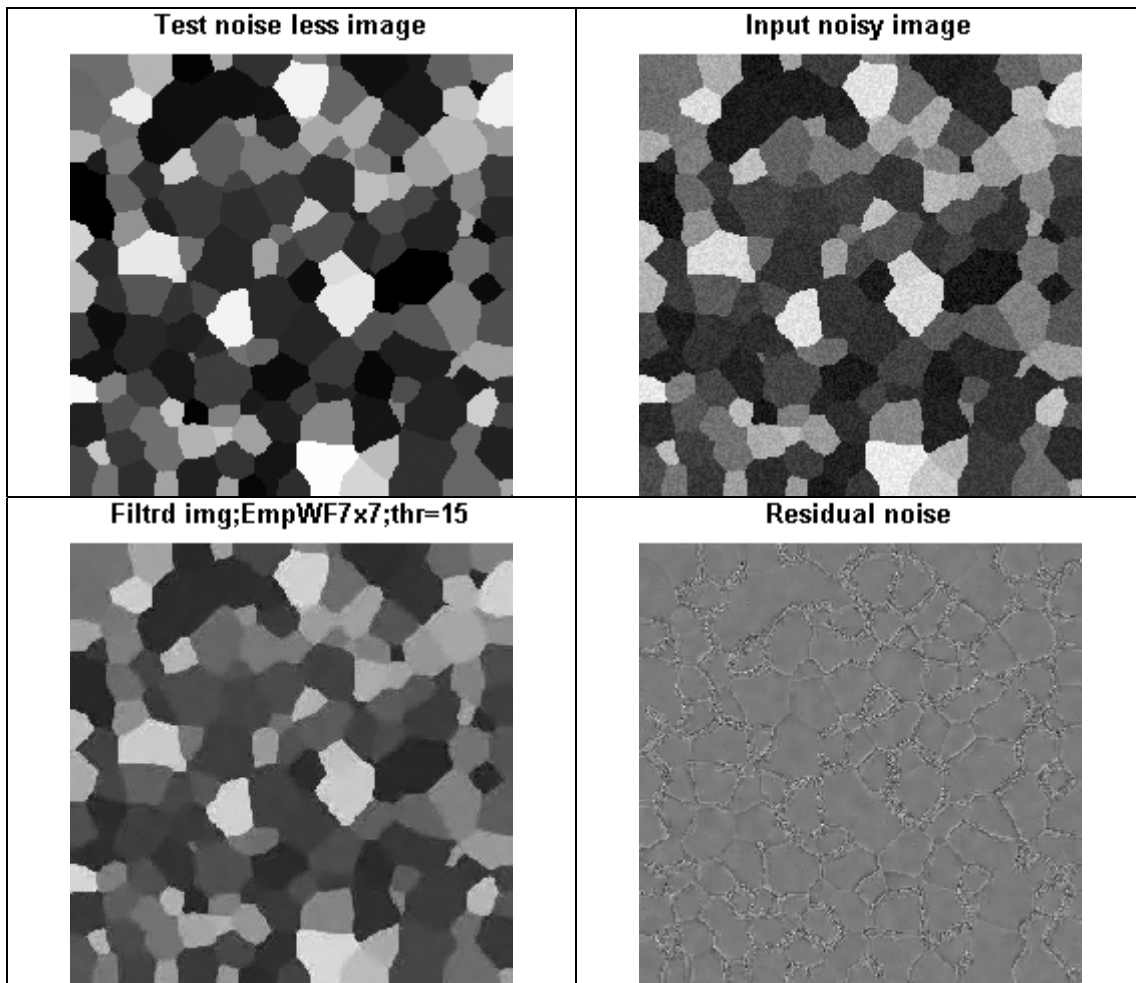


Figure 10.10. Sliding window DCT domain denoising: test image (upper left) noisy test image (upper right), filtered image (bottom left) and residual noise (bottom right).

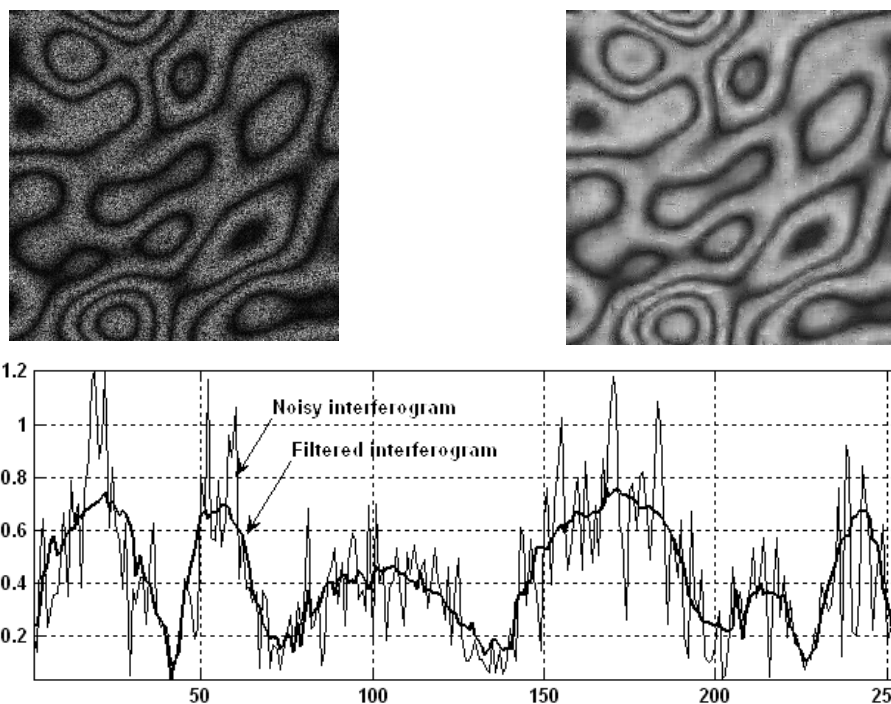


Figure 10.11. An example of local adaptive filtering speckle noise in interferogram: Initial noisy interferogram (upper left), filtered interferogram (upper right) and plots of a typical row of noisy and filtered interferograms

10.5. Methods for correcting image gray scale nonlinear distortions

In the imaging system model introduced in Lect. 9, gray scale distortions are attributed to the point-wise nonlinear transformation unit. Usually in correcting gray scale distortions noise described by the stochastic transformations is ignored. In such an assumption, for correcting image nonlinear transformations in imaging systems it is sufficient to apply to images the corresponding inverse transformation. However, in digital processing one should take into account quantization effects and the fact that any nonlinear transformation of quantized signals results in reducing the number of signal quantization levels. The phenomenon of slinging quantization levels together as the result of their nonlinear transformation is illustrated in Fig. 10.12.

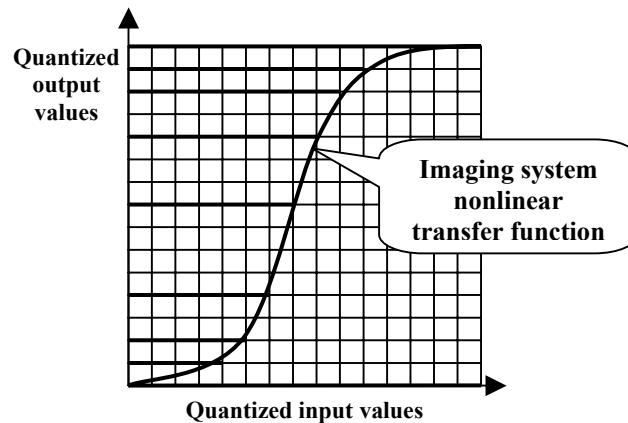


Figure 10.12. Nonlinear signal transformation and the phenomenon of slinging quantization together levels. Thin lines on the figure indicate 16 uniform quantization intervals. The curve shows transfer function of a nonlinear transformation. Bold lines indicate 9 quantization levels left after the nonlinear transformation of 16 quantization levels of input values

For generating correcting nonlinear transformations that can be applied to quantized distorted input signal, methods of signal optimal scalar quantization ([1]) should be applied. Assume that signal quantization is based on the companding-expanding principle. According to this principle,

- at the quantization stage, initial non-quantized signals are first nonlinearly transformed by a companding transformation and then the resulting signals are uniformly quantized;
- at the stage of signal restoration, uniform quantization levels are nonlinearly corrected using a corresponding nonlinear expanding transformation.

Consider now a diagram shown in Fig. 10.13 that explains principle of correcting signal nonlinear distortions in a nonlinear quantization scheme. Let, for the beginning, the nonlinear imaging system transfer function to be corrected (upper right quadrant of the diagram) as well as nonlinear compressing and expanding functions used for signal non-uniform compressor-expander quantization (upper left and bottom right quadrant of the diagram) be known. Project boundaries of quantization intervals of the uniform quantizer (left horizontal coordinate axis) at the output of the compressing transformation to its input (upper vertical coordinate axis) and then further to the input of the nonlinear transformation to be corrected (right horizontal coordinate axis), as it is indicated by arrows in upper left and upper right quadrants of the diagram in Fig. 10.13. This provides boundaries of the quantization intervals of the perfect signal that has to be restored from the distorted and quantized input signal. Within these boundaries, find now optimal quantized representative values of the perfect signal, which minimize the quantization error (dots on the right horizontal coordinate axis).

Finally, project these values back to the input scale of the expanding transformation as indicated by arrows in bottom right quadrants of the diagram. Obtained values determine the needed output values of the correcting look up table (shown by bold circles in the diagram) that have to be assigned to quantized values of the distorted signal.

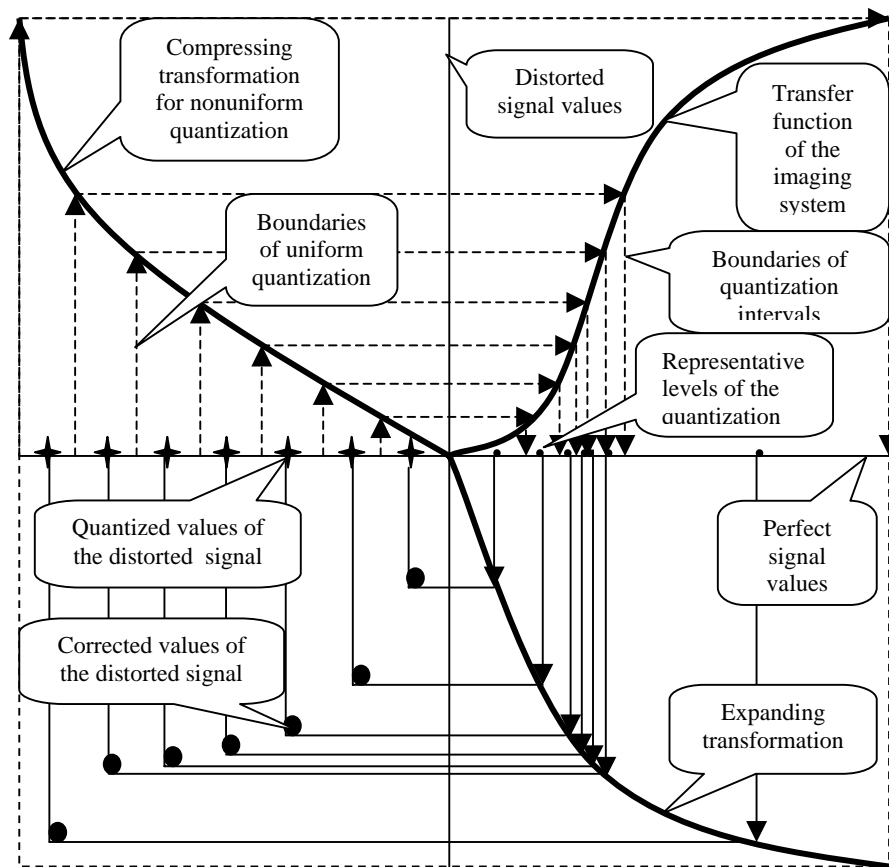


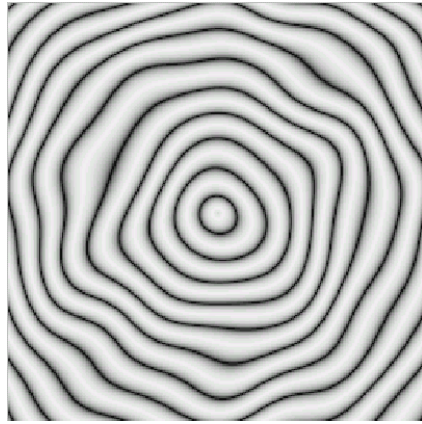
Figure 10.13. Principle of correcting nonlinear distortions with an account for effects of quantization

In applications, it very frequently happens that the nonlinear signal distortion transfer function that has to be corrected is not known. In some cases it can be determined directly from an analysis of the distorted signal. A typical example to illustrate such an opportunity is correcting nonlinear distortions of photographic recording of interferograms.

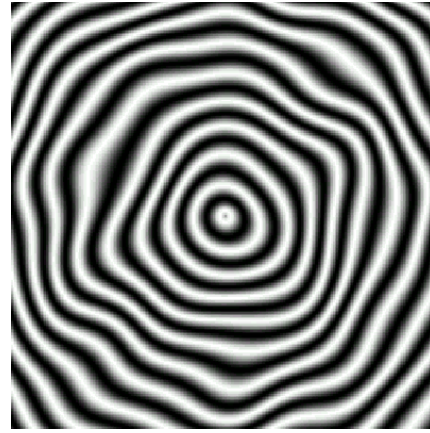
Perfect interferogram signal is a phase modulated sinusoidal signal. If, as it usually happens, the interferogram to be corrected contains many periods of the sinusoidal signal, distribution function of its phase can be regarded to be uniform. One can analytically compute the distribution function of a sinusoidal signal with uniformly distributed phase. Therefore, the correcting nonlinear transformation can be found as a transformation that converts the histogram of the distorted interferogram into the histogram defined by the distribution function of the sinusoidal signal with uniformly distributed phase. We will refer to such a transformation as **histogram matching**. Fig. 10.14 illustrates an example of the histogram matching for correcting nonlinear distortions of an interferogram.

Algorithmically, the histogram matching can be implemented through the **histogram equalization**, a nonlinear transformation that converts images with whatever gray level histograms into images with a uniform histogram ([1]). For the histogram matching, it is sufficient to find a histogram equalization transformation for

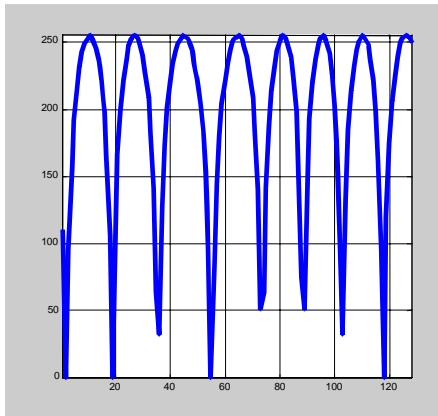
image to be transformed and that for the image with the target histogram. The required histogram matching transformation can then be obtained by combining histogram equalization transformation for the image to be transformed and the transformation inverse to the histogram equalization transformation for the target histogram.



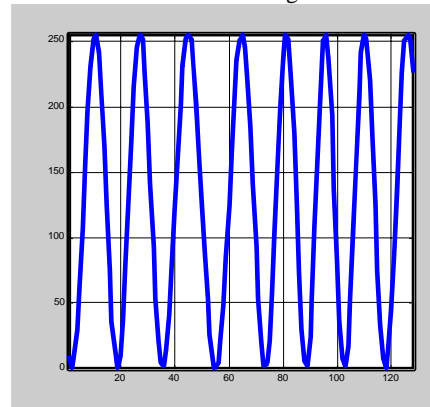
Interferogram with distorted gray scale



Corrected interferogram



Graph of the left half of the central row of the distorted interferogram



Graph of the left half of the central row of the corrected interferogram

Figure10.14. An example of correcting unknown nonlinear distortion of an interferogram

References

1. L. Yaroslavsky, Digital Holography and Digital Image Processing, Kluwer Academic Publishers, Boston, 2004
2. L. Yaroslavsky, Space Variant and Adaptive Transform Domain Image and Video Restoration Methods, In: Advances in Signal transforms: Theory and Applications, J. Astola, L. Yaroslavsky, Eds. , EURASIP Book Series on Signal Processing and Communications, Hindawi, 2007
3. D.L. Donoho and I.M. Johnstone, Ideal Spatial Adaptation by Wavelet Shrinkage, Biometrika, 81(3): 425-455, 1994
4. L. Yaroslavsky, N. Merzlyakov, Methods of Digital Holography, Consultant Bureau, N.Y., 1980
5. M. D. Levine, Vision in Man and Mashine, McGraw-Hill, 1985, pp. 110-130